ENZYME STRUCTURE

Crystal structure of a key enzyme for anaerobic ethane activation

Cedric J. Hahn[1]†, Olivier N. Lemaire[1]†, Jörg Kahnt[2], Sylvain Engilberge[3]‡, Gunter Wegener[1,4,5]*, Tristan Wagner[1]*

Ethane, the second most abundant hydrocarbon gas in the seafloor, is efficiently oxidized by anaerobic archaea in syntrophy with sulfate-reducing bacteria. Here, we report the 0.99-angstrom-resolution structure of the proposed ethane-activating enzyme and describe the specific traits that distinguish it from methane-generating and -consuming methyl-coenzyme M reductases. The widened catalytic chamber, harboring a dimethylated nickel-containing F_{430} cofactor, would adapt the chemistry of methyl-coenzyme M reductases for a two-carbon substrate. A sulfur from methionine replaces the oxygen from a canonical glutamine as the nickel lower-axial ligand, a feature conserved in thermophilic ethanotrophs. Specific loop extensions, a four-helix bundle dilatation, and posttranslational methylations result in the formation of a 33-angstrom-long hydrophobic tunnel, which guides the ethane to the buried active site as confirmed with xenon pressurization experiments.

Natural seeps perfuse the marine seafloor with a variety of different hydrocarbons, including alkane gases (1, 2). Most of the volatile fraction is consumed within the sediment by a process coupled to the reduction of sulfate (2–6), which is mainly carried out by consortia of anaerobic alkane–oxidizing archaea and sulfate-reducing bacteria (5–11). The oxidation of the generated sulfide represents the basis of light-independent ecosystems in the deep sea (6–10, 12). Ethane is the second-most abundant gaseous alkane, but its natural emissions from sediments are estimated to be rather low (2). This low emission results from efficient metabolism of microorganisms that consume the ethane within the seafloor. Recent discoveries pointed out two archaeal species that activate and completely oxidize ethane under anoxic conditions: *Candidatus* Argoarchaeum ethanivorans (7) and *Candidatus* Ethanoperedens thermophilum (8). These two closely related species belonging to the GoM-Arc1 clade are widely present in marine subsurface sediments (5, 7, 8). Analogously to the anaerobic oxidation of methane (AOM), the ethanotrophs generate ethyl-coenzyme M from ethane and coenzyme M (HS-CoM). It has been proposed that such activation works in the same fashion in other alkane-oxidizing archaea (5, 11, 13). It is assumed that ethyl-CoM is further metabolized to acetyl-coenzyme A (acetyl-CoA) by a so-

far-unknown process (7, 8). The acetyl-CoA decarbonylase–synthase complex turns acetyl-CoA into CO_2 and methyl-H_4MPT, and the methyl group is oxidized to CO_2. These organisms depend on ethane as substrate and are incapable of metabolizing other alkanes (7, 8). Generated electrons are transferred to the partner bacteria, supposedly through external cytochromes, nanowires, or diffusible sulfur species, as already discussed for consortia performing the AOM (7, 8, 14, 15).

The central enzyme for alkane-activation in ethanotrophs was proposed to be the methyl-CoM reductase (MCR) (7, 8, 16–18). Extensively studied in methanogens, MCR harbors a specific Ni-porphinoid F_{430} cofactor that catalyzes the reduction of a CoM-bound methyl group with coenzyme B (HS-CoB), forming methane and the heterodisulfide CoM-S-S-CoB (16, 19, 20). The anaerobic methane–oxidizing archaea (ANME) reverse the methanogenesis pathway, using MCR to activate methane, forming methyl-CoM and HS-CoB (21, 22). MCR produced by the ANME-2 clade contains the canonical F_{430} cofactor, whereas a methyl-thio-F_{430}-cofactor was found in MCR from the ANME-1 clade (23–25). The MCR-homolog from ethanotrophs would capture ethane and generate ethyl-CoM and HS-CoB. This hypothesis is corroborated by three observations: (i) genes coding for the three subunits of the MCR-homolog are among the most expressed (7, 8); (ii) ethyl-CoM was formed during anaerobic oxidation of ethane (AOE) by the consortium when incubated in the presence of ethane (7, 8); and (iii) MCR from methanogenic archaea was shown to generate ethane from ethyl-CoM and HS-CoB, yet with rates much lower than for methane generation from methyl-CoM (26, 27). The alkane capture machinery in *Ca.* E. thermophilum appears to be specialized for ethane; ethyl-CoM was the only detectable alkyl-CoM in cells incubated with a

mixture of different alkanes (8). Moreover, in ethanotrophs the protein sequences of the MCR subunits are substantially different from methanogenic MCRs, with large insertions and substitutions of canonical residues (fig. S1 and table S1). Understanding the specific structural features of this enzyme may explain how MCR was adapted to accommodate ethane.

To obtain material for MCR-homolog structure determination, we used a thermophilic AOE enrichment cultured from sediments collected at the Guaymas Basin hydrothermal vents (8). The culture has a doubling time of only 7 days (8), which is notable compared with thermophilic AOM cultures isolated from the same site that exhibit doubling times of 50 days (10). *Ca.* E. thermophilum and its sulfate-reducing bacterial partner, *Candidatus* Desulfofervidus auxilii, constitute most of the active population of the enrichment (8). When we amended the culture medium with the methyl-CoM analog 2-bromoethane sulfonate (BES), a known inhibitor of alkyl-CoM reductases (16), both ethane consumption and sulfide production decreased, dependent on the amount of BES (Fig. 1A and fig. S2). A control ANME culture showed the same sensitivity at similar BES concentrations (Fig. 1A). The results corroborate the hypothesis of an MCR-like enzyme performing ethane activation.

MCR relative abundance in cell extracts from hydrogenotrophic and methylotrophic methanogens as well as ANME-1, ANME-2, and *Ca.* E. thermophilum were compared (Fig. 1B). Native gel profiles of all methanogens indicate an intense band at a size corresponding to isolated MCR. As expected from previous reports (23, 24), the methanotrophic enrichments exhibit a band attributed as MCR with much stronger intensity compared with that of methanogens, resulting from the overproduction of MCR that characterizes these consortia (28, 29). The profile of *Ca.* E. thermophilum contained a protein at a similar position on the native gel that we confirmed with mass spectrometry to be the MCR-homolog (supplementary materials, materials and methods). Compared with the high relative abundance of MCR in ANME enrichments, the cell extract profile of AOE enrichment appears to have a stronger background, similar to that of pure cultures of methanogens. Such lower MCR abundance could result from the lower energy required for the activation of CH bonds of ethane than of methane (16, 26). This, and the overall higher energy yield of sulfate-dependent ethane oxidation (7, 30), may explain the observed faster growth as compared with those of respective methane-oxidizing cultures.

We purified (fig. S3) and crystallized anaerobically the native MCR from *Ca.* E. thermophilum. The x-ray crystal structure was solved

and refined to 0.99-Å resolution (table S2) and presents an organization similar to the eight structurally characterized homologs of MCR from methanogens and ANME-1 (Fig. 2A and table S1). The MCR of Ca. E. thermophilum has the canonical 2(αβγ) organization and is 20 kDa larger as compared with Methanothermobacter marburgensis, resulting from insertions (α10-18, α90-111, α330-340, β70-95, and γ227-240) found in all three subunits. These insertions are present in the enzymes from other ethanotrophs but absent in those of methanogens and methanotrophs (fig. S4). The insertions are located in the same area of the protein surface and redesign the surface charges without interfering with the HS-CoB tunnel, a hydrophilic cavity that connects the bulk solvent to the catalytic center containing HS-CoM and F_{430} (Fig. 2B and fig. S5). The active site organization and coenzymes position indicate a Ni(II)-inactive state. HS-CoM and HS-CoB are present at full occupancy. Most of the residues involved in HS-CoM and HS-CoB binding are conserved with other MCRs, with the exception of the αAla[259] and γTyr[120], which are perfectly conserved in ethanotrophs, replacing the canonical arginine and leucine to position the carboxy-group of HS-CoB and sulfonate-group of HS-CoM, respectively (figs. S1, S4, and S6).

The core of the enzyme embeds the Ni-porphinoid F_{430}-cofactor, exhibiting two methylations of the carbon backbone according to the unambiguous electron density (Fig. 2C). Mass spectrometry and hydrolytic profile confirmed the presence and the position of these methylations (figs. S7 and S8). A gene (locus FHEFKHOI_00788) annotated as a putative uroporphyrinogen-III C methyltransferase and accompanying the coding sequence of the cofactor F_{430} synthetase (cfbE) (31, 32) could be a candidate for the methylation of F_{430} (fig. S9). Sequence alignment and phylogenetic analysis indicate that this gene is an additional copy of the cobM gene, which is specific to ethanotrophs (fig. S9C). The protein encoded by the locus FHEFKHOI_00788 groups in a distinct branch of the CobM methyltransferase phylogenetic tree (fig. S9C). The second homolog branches with CobM sequences from other alkanotrophs and methanogens.

The ultraviolet (UV)–visible spectrum of the purified protein exhibits a different pattern with a maximal absorption peak at 441.5 nm, compared with 424.0 nm for a methanogenic MCR (Fig. 2D). We extracted the dimethylated-F_{430} from the protein to evaluate whether the differences in the spectra are due to the cofactor modifications or a specific protein environment. The extracted dimethylated-F_{430} showed a maximal absorbance at 432.6 nm, thus shifted compared with the classical F_{430}, which has a maximum at 430.4 nm (Fig. 2E). Hence, the observed shift of protein-bound F_{430} mostly
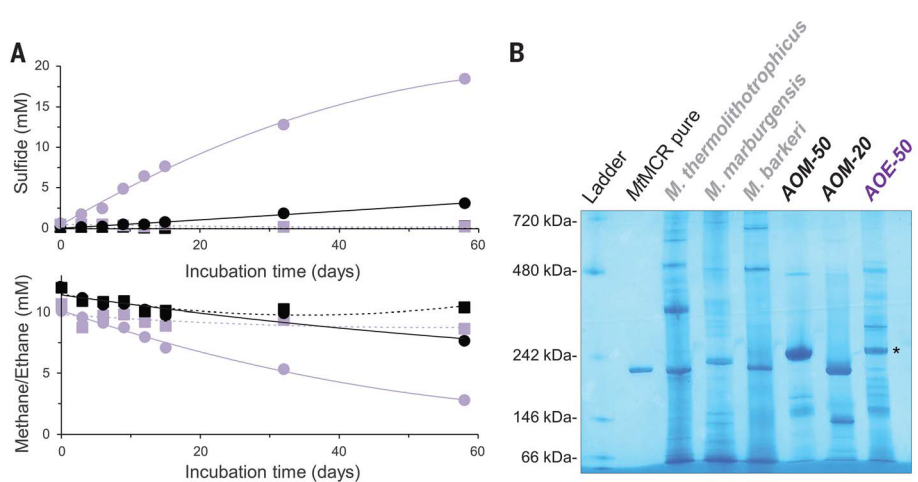

Fig. 1. Inhibition of AOE and comparison of cell extracts from methanogen cultures and methanotrophic and ethanotrophic enrichments. (A) Sulfide generation and alkane degradation in AOM (black) and AOE (purple) cultures incubated at 50°C, in the absence (circles, full lines) or presence (squares, dashed lines) of the MCR-specific inhibitor 2-bromoethane sulfonate at 10 mM (fig. S2). (B) High-resolution clear native polyacrylamide gel electrophoresis of purified MCR from M. thermolithotrophicus (MtMCR, 1.5 mg) and soluble extracts from hydrogenotrophic (M. thermolithotrophicus and M. marburgensis) and methylotrophic (Methanosarcina barkeri) methanogens, AOM and AOE enrichments (10 μg each). The asterisk indicates the position of the MCR homolog from Ca. E. thermophilum.
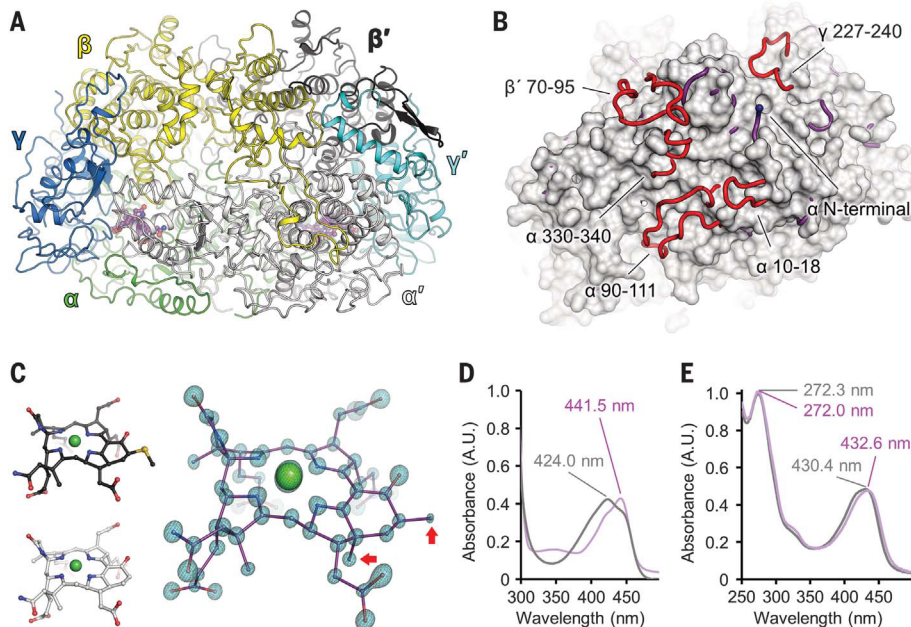

Fig. 2. Structure of the MCR from Ca. E. thermophilum and its dimethylated F_{430}-cofactor. (A) Overall structural organization of the MCR-homolog from Ca. E. thermophilum (PDB 7B1S) represented in cartoon where each subunit harbors a different color code. Prime symbols correspond to the opposing monomers. (B) Superposition of MCR from Ca. E. thermophilum (purple) and MCR type I from M. marburgensis (PDB 5A0Y, white surface) (3). The additional loops in Ca. E. thermophilum (red) are protruding from the M. marburgensis surface. (C) Structure of the cofactor F_{430} from M. marburgensis (white) (33), the methylthio-F_{430} of ANME-1 from Black Sea mats (PDB 3SQG, black) (28), and the dimethylated-F_{430} from Ca. E. thermophilum (purple). The green ball represents nickel, and the methylations are indicated with red arrows. The $2F_o-F_c$ map is contoured at 6σ and shown as a transparent blue surface with a black mesh. (D) UV-visible spectra of MCRs (both at 78 μM concentration) and (E) the extracted F_{430} (normalized for comparison) from Ca. E. thermophilum (purple) and M. thermolithotrophicus (gray).

results from differences in its coordination in the enzyme rather than its methylations.

Contrary to all structurally characterized MCRs, the enzyme from *Ca.* E. thermophilum coordinates the nickel by means of a methionine instead of the canonical glutamine. The sulfur from the methionine interacts with the nickel without disturbing the metal position in the porphinoid ring (Fig. 3, A and B, and fig. S10). The methionine substitution cannot be considered as a prerequisite for ethane activation because the canonical glutamine is conserved in the MCR of the ethane oxidizer *Ca.*

A. ethanivorans and relatives from cold seep environments (figs. S1 and S4). MCRs from methanogens and ANME archaea have virtually identical active sites, illustrating the selective pressure on the residues necessary for this complicated reaction (fig. S11, A and B) (*16*, *23*). It is therefore noteworthy to observe a different composition of the active site in the MCR-homolog from ethane oxidizers (Fig. 3C). The most notable differences are in the loop α367-374, carrying the bulky αTrp[373] that replaces the canonical phenylalanine. This loop displaced the porphinoid ring owing to hydro-

gen bond network from the αAsn[375] and accompanied by a clamping effect from αTyr[376] and αPhe[441], causing a tilting of the ring by 11.4° compared with other MCRs (Fig. 3C and fig. S11B). As a result, the distance between the thiol groups of HS-CoM and HS-CoB is the longest reported so far in inactive Ni(II) structures of MCRs, with 6.6 Å compared with the 6.3 Å on average (Fig. 3, A and B). The catalytic chamber gains in volume (Fig. 3, D and E, and fig. S11, C and D), allowing ethane binding through appropriate van der Waals interactions. The chamber widening could impair the correct positioning of a classic cofactor F_{430} on the protein scaffold (Fig. 3, C to E, and fig. S11). However, the additional methylations on the F_{430} would structurally overcome this issue by maintaining its correct position and the integrity of the porphinoid planarity. We propose that these methylations accommodate the cofactor in this dilated active site and assure its appropriate environment to maintain its reactivity (Fig. 3, C to E).

The structure of MCR from *M. marburgensis* revealed a spherical electron density between the thiols of HS-CoM and HS-CoB (*16*). Similarly, the MCR of *Ca.* E. thermophilum has a weak elongated electron density at this position. The modeling of a diatomic molecule such as ethane would be preferred to a water molecule, albeit static disorder in the cavity could also lead to the observed density (fig. S12). To confirm the ethane-binding site and characterize a putative path inside the enzyme, we performed a xenon-pressurization experiment. Across the whole MCR from *Ca.* E. thermophilum, 16 Xe sites were unambiguously detected (fig. S13 and table S3). The major Xe site was found at the ethane site, between the two coenzymes, without interfering with the thiol groups. A second site was detected in a hydrophobic cavity located between the active site and the surface. Computational analysis confirmed that this cavity is part of an extended tunnel of 33 Å length (Fig. 4). According to the atomic-resolution structure, the tunnel is devoid of water molecules, attesting to its hydrophobic properties, which are ideal for the diffusion of hydrophobic gases such as ethane. All other Xe sites were found on the surface in hydrophobic pockets. No Xe was detected in the coenzyme tunnel because the proteins in the crystal systematically contain both HS-CoM and HS-CoB, preventing Xe diffusion into the tunnel. A similar computational analysis did not detect a similar tunnel in MCRs from *M. marburgensis* and ANME-1.

The MCR from *M. marburgensis* can generate ethane from ethyl-CoM and HS-CoB, albeit with low affinity and activity compared with methane production (*26*, *27*). Xenon-pressurization of crystals from *M. marburgensis* MCR isoform I [named type I, in reference to (*33*)] revealed 12 Xe sites exclusively located
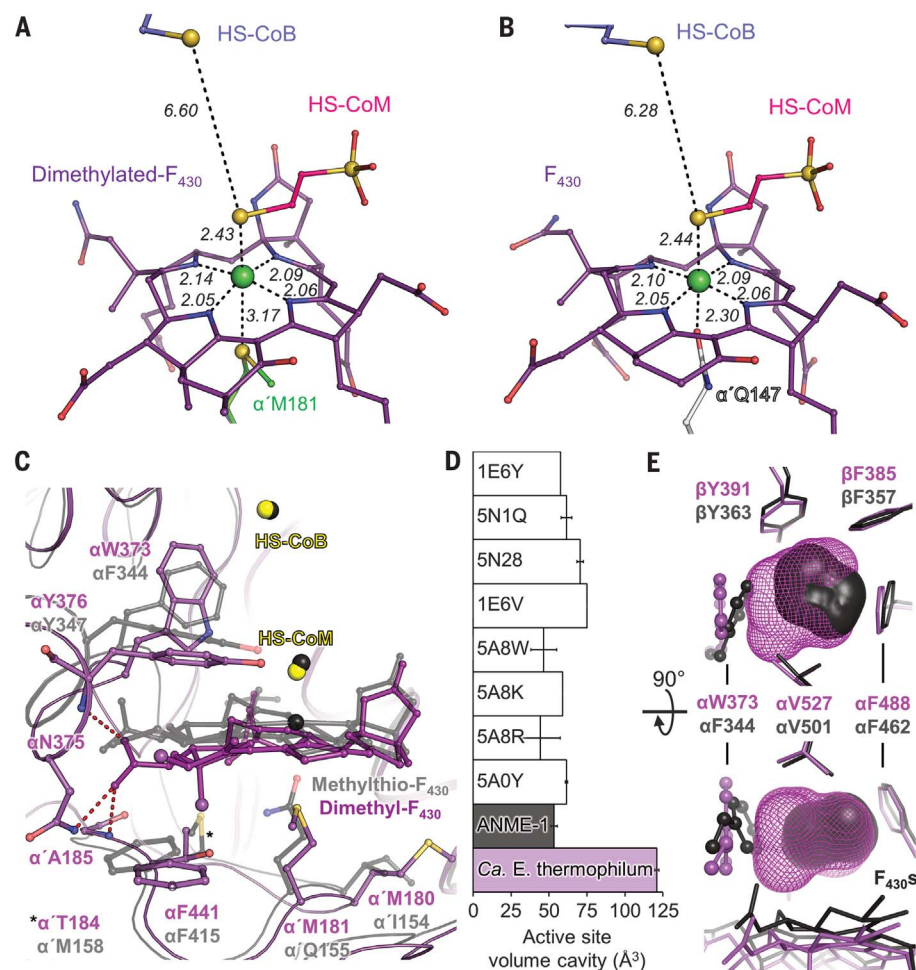

Fig. 3. A widened active site to accommodate ethane. (**A** and **B**) Nickel coordination in atomic resolution structures of *Ca.* E. thermophilum [(A), PDB 7B1S] and MCR type I from *M. marburgensis* [(B), PDB 5AOY]. Distances between the nickel (green ball) and its surrounding atoms are indicated with dashes and given in angstroms. (**C**) Cartoon representation of MCR from ANME-1 (transparent black, with nickel as ball, PDB 3SQG) superposed on the C terminus of the α-subunit of *Ca.* E. thermophilum (purple). HS-CoM, HS-CoB reactive thiols are shown as balls. F_{430}s and residues involved in the tilting of the dimethylated-F_{430} are shown as balls and sticks, and hydrogen bonds are indicated with red dashes. Most ethanoic and propanoic groups of the F_{430}s and water network were omitted for clarity. (**D**) Volume of each of the catalytic cavities in MCR structures from methanogens (white, indicated by PDB codes) (supplementary materials, materials and methods), methanotroph (black), and ethanotroph (purple) are reported on the histogram. (**E**) Comparison of the catalytic cavity volume between MCR from ANME-1 (black surface) and *Ca.* E. thermophilum (purple mesh). Surrounding residues are shown as sticks. The αTrp[373] position is indicated with balls and sticks.
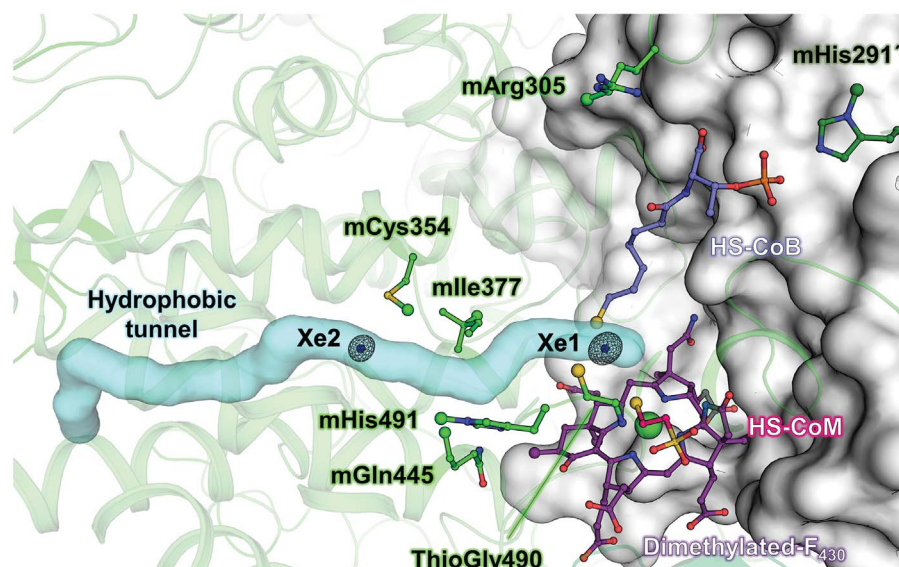
Fig. 4. Ethane tunnel supporting gas diffusion toward the catalytic chamber. The protein is displayed in cartoon, with the α′-subunit as white surface. Posttranslational modifications, cofactor, and coenzymes are shown in sticks, with additional methyls and sulfurs as green and yellow balls, respectively. The hydrophobic tunnel calculated by the CAVER program (*34*) creating a route for the substrate to the catalytic center of the enzyme is shown as a cyan surface. The anomalous Fourier map contoured at 15σ shown as black mesh indicates the position of Xe atoms obtained with xenon-pressurization experiment (PDB 7B2C), indicated with dark blue spheres.

at the surface of the enzyme in hydrophobic pockets (fig. S14 and table S3), and no Xe could be detected in the catalytic chamber. These results suggest that the internal tunnel is specific to ethane oxidizers and could allow for efficient transport of ethane to the catalytic center. In *Ca.* E. thermophilum, the tunnel is formed at the interface of a four-helix bundle from the α subunit (helices 340-367, 373-382, 443-463, and 527-544). It is covered and flanked at the outer surface by the specific additional loops and the helix 385-401 (fig. S15). The opposite side of the tunnel, opening in the active site, is covered with posttranslationally modified residues: S-methylcysteine-354, 3-methylisoleucine-377, 2(*S*)-methylglutamine-445, and N^2-methylhistidine-491 (Fig. 4 and figs. S15 and S16). The N^2-methylhistidine-491 is of particular interest because this residue is a tyrosine or phenylalanine in all other MCRs (figs. S1 and S4). Installation of these modifications would require a specific machinery that will need further investigation. Other modifications systematically found in methane-releasing MCRs were detected in the electron density and confirmed with mass spectrometry (fig. S16).

Our results reveal specific structural features harbored by the MCR-homolog of the ethane oxidizer *Ca.* E. thermophilum, which favors ethane consumption over methane or larger alkanes (*8*). We propose to rename this enzyme, which is the entry point for anaerobic oxidation of ethane, to ethyl-CoM reductase (ECR). Assuming a similar organization of the active Ni(I) enzyme, the larger volume of the catalytic cavity would likely impair correct positioning of methane. The chamber volume would not be sufficient to accommodate alkanes larger than ethane, especially in the heterodisulfide-containing enzyme. Moreover, the hydrophobic tunnel inner diameter (average bottleneck radius 1.02 Å) would already prevent more voluminous alkanes such as propane from accessing the active site. Future investigations should resolve how the ECR active site constrains a particular reactive state of the ethane, allowing its exclusive and efficient capture.

REFERENCES AND NOTES

1. J. F. Clark, L. Washburn, J. S. Hornafius, B. P. Luyendyk, *J. Geophys. Res.* **105** (C5), 11509–11522 (2000).
2. G. Etiope, P. Ciccioli, *Science* **323**, 478–478 (2009).
3. S. B. Joye et al., *Chem. Geol.* **205**, 219–238 (2004).
4. V. Mastalerz, G. J. de Lange, A. Dahlmann, *Geochim. Cosmochim. Acta* **73**, 3849–3863 (2009).
5. R. Laso-Pérez et al., *mBio* **10**, e01814–e01819 (2019).
6. A. Boetius et al., *Nature* **407**, 623–626 (2000).
7. S. C. Chen et al., *Nature* **568**, 108–111 (2019).
8. C. J. Hahn et al., *mBio* **11**, e00600–e00620 (2020).
9. V. J. Orphan, C. H. House, K. U. Hinrichs, K. D. McKeegan, E. F. DeLong, *Science* **293**, 484–487 (2001).
10. T. Holler et al., *ISME J.* **5**, 1946–1956 (2011).
11. R. Laso-Pérez et al., *Nature* **539**, 396–401 (2016).
12. M. Sibuet, K. Olu, *Deep Sea Res. Part II Top. Stud. Oceanogr.* **45**, 517–567 (1998).
13. G. Borrel et al., *Nat. Microbiol.* **4**, 603–613 (2019).
14. S. E. McGlynn, G. L. Chadwick, C. P. Kempes, V. J. Orphan, *Nature* **526**, 531–535 (2015).
15. G. Wegener, V. Krukenberg, D. Riedel, H. E. Tegetmeyer, A. Boetius, *Nature* **526**, 587–590 (2015).
16. R. K. Thauer, *Biochemistry* **58**, 5198–5220 (2019).
17. D. V. Miller, S. J. Booker, *Biochemistry* **58**, 4269–4271 (2019).
18. Y. Wang, G. Wegener, S. E. Ruff, F. Wang, *Environ. Microbiol.* **23**, 530–541 (2021).
19. U. Ermler, W. Grabarse, S. Shima, M. Goubeaud, R. K. Thauer, *Science* **278**, 1457–1462 (1997).
20. T. Wongnate et al., *Science* **352**, 953–958 (2016).
21. S. J. Hallam et al., *Science* **305**, 1457–1462 (2004).
22. A. Meyerdierks et al., *Environ. Microbiol.* **12**, 422–439 (2010).
23. S. Shima et al., *Nature* **481**, 98–101 (2011).
24. M. Krüger et al., *Nature* **426**, 878–881 (2003).
25. M. Kaneko et al., *Anal. Chem.* **86**, 3633–3638 (2014).
26. S. Scheller, M. Goenrich, R. K. Thauer, B. Jaun, *J. Am. Chem. Soc.* **135**, 14985–14995 (2013).
27. R. P. Gunsalus, J. A. Romesser, R. S. Wolfe, *Biochemistry* **17**, 2374–2377 (1978).
28. F. P. Wang et al., *ISME J.* **8**, 1069–1078 (2014).
29. V. Krukenberg et al., *Environ. Microbiol.* **20**, 1651–1666 (2018).
30. R. K. Thauer, *Curr. Opin. Microbiol.* **14**, 292–299 (2011).
31. K. Zheng, P. D. Ngo, V. L. Owens, X. P. Yang, S. O. Mansoorabadi, *Science* **354**, 339–342 (2016).
32. S. J. Moore et al., *Nature* **543**, 78–82 (2017).
33. T. Wagner, J. Kahnt, U. Ermler, S. Shima, *Angew. Chem. Int. Ed.* **55**, 10630–10633 (2016).
34. E. Chovancova et al., *PLOS Comput. Biol.* **8**, e1002708 (2012).
35. Hahn et al., X-ray crystallography and mass spectrometry raw and processed data accompanying the manuscript "Crystal structure of a key enzyme for anaerobic ethane activation". Zenodo (2021).

SUPPLEMENTARY MATERIALS

science.sciencemag.org/content/373/6550/118/suppl/DC1
Materials and Methods
Supplementary Text
Figs. S1 to S16
Tables S1 to S3
References (*36*–*58*)

View/request a protocol for this paper from *Bio-protocol*.

Science

Crystal structure of a key enzyme for anaerobic ethane activation

Cedric J. Hahn, Olivier N. Lemaire, Jörg Kahnt, Sylvain Engilberge, Gunter Wegener and Tristan Wagner

How to feed an enzyme ethane

When released from ocean floor seeps, small hydrocarbons are rapidly consumed by micro-organisms. Methane is highly abundant and is both produced and consumed by microbes through well understood biochemical pathways. Less well understood is how ethane, also a major natural component of gaseous hydrocarbons, is metabolized. To understand how microbes take advantage of this energy and carbon source, Hahn *et al.* solved the x-ray crystal structures of an enzyme they call ethyl coenzyme-M reductase, which converts ethane into the thioether ethyl-coenzyme M as the entry point for catabolism. They found an expanded active site and, using a xenon gas derivatization experiment, a distinctive tunnel through the protein that is proposed to permit access of the gaseous substrate.
Science, abg1765, this issue p. 118